Optimizing spinal cord injury in zebrafish larvae: effects of age on the injury response

Kirsten L. Underwood,[1†] Whitney J. Walker,[1,2†] Patrick I. Garrett,[3,4]
Shannon Linch,[1] Thomas P. Rynes[1] and Karen Mruk[1,3,4*]

[1]School of Pharmacy, University of Wyoming, Laramie, WY, USA
[2]Zoology and Physiology Graduate Program, University of Wyoming, Laramie, WY, USA
[3]Neurosciences Graduate Program, University of Wyoming, Laramie, WY, USA
[4]Department of Pharmacology and Toxicology, Brody School of Medicine, East Carolina University, Greenville, North Carolina, USA.

[†]These authors contributed equally to this work.

*Address correspondence to:

Dr. Karen Mruk
East Carolina University
Brody School of Medicine
Department of Pharmacology and Toxicology
600 Moye Boulevard
Greenville, NC 27834
Tel: 252-744-1171
Email: mrukk23@ecu.edu

ABSTRACT

Zebrafish are an increasingly popular model to study spinal cord injury (SCI) regeneration. The transparency of larval zebrafish makes them ideal to study cellular processes in real time. Standardized approaches, including age of injury, are not readily available making comparisons of the results with other models challenging. In this study, we systematically examined the response to spinal cord transection of larval zebrafish at three different ages (3-7 days post fertilization or dpf) to determine whether the developmental complexity of the central nervous system affects the overall response to SCI. We then used imaging and behavioral analysis to evaluate whether differences existed based on the age of injury. All ages of larval zebrafish upregulated the required genes for glial bridge formation, *ctgfa* and *gfap,* at the site of injury, consistent with studies from adult zebrafish. Though all larval ages upregulated factors required to promote glial bridging, young larval zebrafish (3 dpf) were better able to regenerate axons independent of the glial bridge, unlike older zebrafish (7 dpf). Consistent with this data, locomotor experiments demonstrated that some swimming behavior occurs independent of glial bridge formation, further highlighting the need for standardization of this model and recovery assays. Overall, we found subtle cellular differences based on the age of transection in zebrafish, underlining the importance of considering age when designing experiments aimed at understanding regeneration.

KEYWORDS

functional recovery, development, spinal cord transection

INTRODUCTION

Spinal cord injury (SCI) is a devastating event that leads to permanent loss of function in mammals. The zebrafish central nervous system (CNS) shares many organizational, cellular and molecular pathways with mammals including myelinated axons (Brösamle and Halpern, 2002) and use of the same neurotransmitters (Panula et al., 2006). Despite these similarities, regeneration and locomotor recovery occur in zebrafish even after complete transection of the spinal cord (van Raamsdonk et al., 1998). Understanding the similarities and differences between regenerative zebrafish and non-regenerative mammals could be pivotal for identifying new therapeutic targets and strategies to induce functional recovery in humans.

Adult zebrafish retain their regenerative ability through their lifetime, making them an obvious choice to compare with mammalian models. However, adult zebrafish take longer to recover (Vajn et al., 2014) and require complicated surgical procedures (Fang et al., 2012), which preclude the use of this model from many laboratories with smaller facilities that cannot support the animal number or specialized techniques required for adult zebrafish studies. Furthermore, adult zebrafish are not optically transparent, limiting the use of real-time imaging of cellular processes during regeneration.

Larval zebrafish offer many experimental advantages over adult zebrafish to study SCI (Alper and Dorsky, 2022). Most notably, larval zebrafish offer a transparent model to study regeneration in real time. Many processes are conserved between larval and adult zebrafish. Studies demonstrated that innate immune cells infiltrate the injury site in both larvae (Cavone et al., 2021; Gollmann-Tepeköylü et al., 2020; Tsarouchas et al., 2018) and adults (Hui et al., 2010; Hui et al., 2014) and are required for regeneration. SCI in both larvae (Ohnmacht et al., 2016) and

adults (Reimer et al., 2013) leads to regeneration of motor neurons, which is enhanced through dopamine agonism. Lastly, both larval and adult zebrafish form a glial bridge across the injury site (Briona and Dorsky, 2014a; Goldshmit et al., 2012; Klatt Shaw et al., 2021; Matsuoka et al., 2016; Mokalled et al., 2016) which may promote axon growth after SCI. Although each of these studies highlights the utility of the larval model, differences in injury methods and the age used for experiments limits the interpretation of these studies when compared with adults or mammals.

Embryonic development is classically defined as ending at the time of hatching, 3–4 days post fertilization (dpf) (Kimmel et al., 1995; Parichy et al., 2009) with larval development continuing for approximately six weeks. Often laboratories use late embryonic and early larval stages due to ease and ethical considerations (Tsarouchas et al., 2018) with some studies looking at larvae as old as 10 dpf (Hossainian et al., 2022). Furthermore, neurogenesis of primary motor neurons is greatly reduced at 2 dpf (Reimer et al., 2013) and nascent myelin is observed 3-4 dpf (Bin and Lyons, 2016; Kirby et al., 2006; Park et al., 2002; Preston and Macklin, 2015). Although injury-dependent mechanisms have been identified in these earlier ages, these studies can be limiting as additional factors such as mature synaptic connections and myelin debris are largely absent in zebrafish injured this young. We sought to determine whether larvae transected at different ages demonstrated regenerative differences. We transected the spinal cord of larval zebrafish at 3 dpf, 5 dpf, and 7 dpf and characterized the subsequent cellular events and locomotor recovery. We show that mortality rate and secondary injury depend on the age of injury. We also observed differences in axonal bridging and swim behavior with age. Taken together, our data suggests that age should be considered when designing larval zebrafish SCI experiments.

RESULTS

Age-dependent survival and secondary injury in zebrafish larvae

Previous studies have reported up to 50% mortality using mechanical transection in larval zebrafish (Bhatt et al., 2004). Therefore, using bright field microscopy, we first determined whether mechanical transection affected larval zebrafish survival after SCI. We transected *Tg(gfap:EGFP)* zebrafish larvae at 3 dpf, 5 dpf, or 7 dpf and used the signal from green fluorescent protein (EGFP) to confirm the presence of a complete transection. We chose these ages as they correlate with end of embryonic stage (Parichy et al., 2009), development of feeding (Hernandez et al., 2018), and mineralization of the centra (Bensimon-Brito et al., 2012). Both age-matched control larvae that were not injured and fully transected larvae were recorded daily for survival from the day of injury through 7 days post injury (7 dpi). In fish cut at 3 dpf, there was a significant decline to 71% survival at 4 dpi (Fig. 1A). Unlike young larvae, feeding larvae (5 dpf) exhibited high survival rates (86%) until 7 dpi (Fig. 1B). Lastly, older larvae (7 dpf) exhibited steady declines in survival for both the control and injured fish (Fig. 1C) resulting in overall survival of 59%.

As other organ systems are still maturing at larval ages (Brown et al., 2016), we wondered whether the collateral damage from a mechanical transection may be causing the changes we observed in survival. We first looked at normal physiological development. In zebrafish, the inner most lining of the swim bladder is formed by 3 dpf, with inflation of the chamber occurring at approximately 4.5 dpf (Winata et al., 2009). After transection, we found that larvae injured at 3 dpf failed to properly inflate swim bladders as late as five days after injury (8 dpf, 22% compared with 96% for control larvae) (Fig. S1A). To ensure this was due to the SCI and not an artifact of the *Tg(gfap:EGFP)* line, we also monitored the inflation of a swim bladder in *Tg(olig2:dsRed*)

larvae and similarly found that swim bladder inflation was reduced (8 dpf, 12% vs. 100% for control larvae) (Fig S1B) indicating that injury affected normal swim bladder development. We also measured the heart rate of individual zebrafish larvae and tracked individual fish over time to determine whether survival of larvae could be predicted (Fig. S1C). Larvae injured at 3 dpf, showed a slight but not statistically significant increase in heart rate at 1 dpi which stayed elevated through 3 dpi. In contrast, larvae injured at 5 dpf showed a decrease in heart rate on the day after injury with larvae injured at 7 dpf showing no differences in heart rate across all ages (Fig. S1C). For all ages, individual larvae with greatly reduced blood flow were most likely to die over the course of the week. Given that the small differences observed in heart rate across ages were not statistically significant, additional cellular mechanisms may be leading to differences in mortality.

There are two mechanisms of damage after SCI: a primary mechanical injury and a secondary injury mediated by many processes including inflammation and continued cell death. In mammals, apoptosis can occur hours after injury and occur in some cell types up to weeks later (Mizuno et al., 1998). To determine the amount of apoptotic cells in the spinal cord after injury, we incubated live *Tg(olig2:dsRed)* larvae with acridine orange from 12 hours post injury (hpi) – 5 dpi. Using the dsRed signal to exclude acridine orange signal from outside of the CNS, we observed day-to-day differences between the ages of injury. For larvae injured at 3 dpf or 5 dpf, we found a significant increase in the number of apoptotic cells at 12 hpi and 24 hpi (Fig. 1D, E) compared to controls. In these larvae, apoptosis began to significantly resolve at 72 hpi (p value for 12 hpi vs 72 hpi = 0.001 and 0.0092 respectively). In contrast, there was no reduction in the number of apoptotic cells among larvae transected at 7 dpf (p value for 12 hpi vs 120 hpi >0.9999), indicating a more sustained secondary injury process (Fig. 1D, E).

GFAP+ cells accumulate differently at the site of injury

A hallmark of the adult zebrafish response to spinal cord injury is the formation of a glial bridge (Goldshmit et al., 2012; Mokalled et al., 2016). Therefore, we next determined whether larval zebrafish faithfully recapitulated glial recovery seen in adult zebrafish. We analyzed the formation of a radial glial bridge in *Tg(gfap:EGFP)* larvae that had a complete spinal cord transection at 3, 5, or 7 dpf. After injury, we observed that larval zebrafish transected at 3 dpf began the bridging process as early as 1 dpi with ~90% of larvae forming a glial bridge by 5 dpi (Fig. S2A). Larval zebrafish transected at 5 dpf and 7 dpf did not begin to bridge until 2 dpi with a lower percentage of bridging overall (Fig. 2A and Fig. S2C). The percentage of bridged zebrafish did not increase when larvae were monitored for longer times suggesting that some injured larvae do not ever form a bridge. As glial bridging could be impacted by the size of the injury, we measured the width of injury and formation of a glial bridge by quantifying GFP pixel intensity. For all ages, the transection width was 100-250 microns indicating the injury size was not the reason for variable bridge formation. For larval zebrafish transected at 3 dpf and 5 dpf, GFP signal accumulated around the site of injury (Fig. 2B and Fig. S2B). Unexpectedly, we found that GFP intensity only accumulated on the rostral side of the injury in larval zebrafish transected at 7 dpf (Fig. S2D). In adult zebrafish, cells at the edge of the lesion express low levels of GFAP (Goldshmit et al., 2012). Therefore, to confirm that the GFP intensity was not due to an increase in *gfap* expression, we used quantitative PCR (qPCR). We found that larval zebrafish transected at 3 dpf and 5 dpf had either reduced or unchanged expression levels of *gfap* until 4 dpi (Table 1). In contrast, older larvae showed relatively stable expression levels of *gfap,* suggesting the increased pixel intensity observed is not just due to increased levels of GFP.

One factor required for glial bridging in adult zebrafish is connective tissue growth factor a (CTGFa) (Mokalled et al., 2016). Using *in situ* hybridization, we found that larval zebrafish express *ctgfa* in the site of injury as early as hours after transection (0 dpi) independent of age (Figure 2C-E). Expression of *ctgfa* was observed over the five-day time course for all ages. We also confirmed upregulation of *ctgfa* using qPCR. We found that independent of transection age, all larvae upregulated *ctgfa* between 2-3 dpi which remained elevated even after glial bridging (Table 1). Taken together, the cellular accumulation of GFAP+ cells differed with age of injury, but the molecular mechanisms governing bridging appears conserved across ages.

Recovery of free swim occurs independently of glial bridging

One aspect of complex behaviors in zebrafish is their ability to move at various speeds, which requires signals coming from the brain and local spinal cord circuitry (Berg et al., 2023; Kishore et al., 2014; Severi et al., 2014). Most groups assay a single property such as total distance; however, larvae can produce similar total distances by generating different swim durations and/or speed Therefore, we used video tracking to analyze swim distance occurring from twitch (0-2 mm/s), small (2-4 mm/s), and large (>4 mm/s) movements. For these studies, we focused on larvae injured at 5 dpf and 7 dpf, given coordinated movement does not begin until 4 dpf (Brustein et al., 2003; Drapeau et al., 2002). Although larval zebrafish transected at 5 dpf and 7 dpf showed a significant decrease in distance generated from all swim speeds compared to uncut controls, the distance recorded from each movement from injured larvae did statistically increase over the week long experiment suggesting swim speed was returning over time (Fig. 3A and Fig. S3A). We next asked whether the observed difference in swim ability at various swim speeds reflects the formation of a glial bridge. On the last day of the experiment, an independent observer imaged the

zebrafish larvae and scored them for the presence of a glial bridge. Fish transected at 5 dpf that formed a glial bridge recovered their swim distance from all swim speeds comparable to uncut controls. However, larvae that did not form a glial bridge did not appreciably recover small or large swim speeds (Fig. 3B). In contrast, fish transected at 7 dpf did not appreciably recover any type of swim speed independent of the glial bridge formation suggesting that age of injury may affect locomotor recovery (Fig S3B).

Axons cross the site of injury independent of a glial bridge

Because recovery of locomotion did not directly correlate with glial bridging, we next examined whether glial bridging correlated with axonal growth across the injury site. We generated heterozygous *Tg(elavl3:mCherry-CAAX)* zebrafish and crossed them with *Tg(gfap:EGFP)* zebrafish to generate larvae which contained labeled neurons and radial glia. Both the sensory and motor tracts are clearly labeled in these larvae (Fig. 4). The advantage of this line permits sequential imaging of the same transected larvae over the course of the experiment instead of relying on fixed larvae for immunohistochemistry. The radial glia in all transected larvae exhibited the well-characterized morphological change (Fig. 4A), of becoming more elongated (Briona and Dorsky, 2014a; Kim et al., 2008; Matsuoka et al., 2016). Fifty percent of larvae transected at 3 dpf formed a glia bridge with axons crossing the site of injury within two days (Fig. 4B). As these larvae aged, we again observed that not all larvae formed a glial bridge (Fig. S4); however, axonal growth continued such that 89% of larvae had axons that crossed the site of injury. Older larvae took longer to form a glial bridge (3 days for 50% of larvae), with larvae cut at 7 dpf having the lowest percentage of axons crossing the site of injury (Fig. 4B).

DISCUSSION

Motivated by the boom of SCI studies in various aged zebrafish, we systematically looked at SCI in three ages of larval zebrafish to identify similarities and differences of the recovery process. Although the process of spinal cord regeneration is distinct from spinal development (Alper and Dorsky, 2022), we observed subtle differences across the different ages of injury, indicating that there is an interplay between development and regeneration. For example, we found swim bladder development was impaired in larvae that were injured young (Fig. S1). This is perhaps unsurprising as both patterning of the spinal cord after injury (Reimer et al., 2009) and swim bladder development (Winata et al., 2009) require sonic hedgehog (Shh) signaling. However, few studies address whether and how resources are prioritized in developing animals across species to promote regeneration. Our results open the door to new experimental approaches for this model organism, as larvae have many experimental advantages over adult zebrafish. For example, transgenic lines can be used to look at individual larvae such that a specific injury can be monitored from time of injury to regeneration. Most researchers, including ourselves, use the cloaca as a marker for spatial reproducibility (Briona and Dorsky, 2014b; John et al., 2022); however, manual transection can lead to slight differences in extent of injury including: partial transections, size of injury, amount of secondary injury, and extraneous tissue damage (including the notochord). Factors such as how much the injury area expanded are challenging to assay in fixed tissues without a direct comparison to the initial injury.

SCI studies in zebrafish have focused on identifying the molecular drivers of axonal regeneration (Drake et al., 2023; Fang et al., 2014; Garcia et al., 2018; Ghosh and Hui, 2018; Keatinge et al., 2021; Li et al., 2020b; Noorimotlagh et al., 2017), circuit remodeling (Huang et

al., 2022; Huang et al., 2021), glial bridging (Goldshmit et al., 2012; Klatt Shaw et al., 2021; Mokalled et al., 2016), and the immune response (Anguita-Salinas et al., 2019; Tsarouchas et al., 2018; Vandestadt et al., 2021). Our studies take a broad-strokes approach to look at the whole organism during the process of regeneration. This work opens the door to using larval zebrafish to study the mechanisms of known complications of SCI. For example, SCI is associated with cardiac dysfunction in mammals (Grigorean et al., 2009; Partida et al., 2016; Popa et al., 2010), including cardiac dysrhythmias, cardiac arrest, and hypotension. Our results indicate that larval zebrafish may exhibit some of these same dysfunctions (Fig. S1) providing a new model to address SCI complications. Although we did not look at other organ systems, considering the anatomical similarities of the zebrafish to mammals, future studies looking at effects in the urinary (Kolvenbach et al., 2023; Outtandy et al., 2019) and gastrointestinal tract (Flores et al., 2020; Sadler et al., 2013) are warranted.

One unexpected finding was the difference in radial glia accumulation at the site of injury (Fig. 2 and S2). In both adult (Goldshmit et al., 2012) and larvae (Briona and Dorsky, 2014a) zebrafish, Gfap+ cells become elongated and form a bridge across the site of injury. In adults, Gfap+ cells proliferate around the central canal and express low levels of *gfap* (Goldshmit et al., 2012).We also observed an accumulation of Gfap+ cells around the site of injury, in larval zebrafish. These Gfap+ cells adopted an elongated morphology (Fig. 4), but the location of accumulation was dependent on the age of the animal. The primarily rostral accumulation is consistent with where *ctgfa* expression is observed in longitudinal spinal cord sections from injured adult zebrafish (Mokalled et al., 2016). However, despite observing accumulation of GFP signal in all samples, not all samples formed a glial bridge. Taken together these results suggest that there

may be additional signals driving the radial glia response in larval zebrafish based on the age and/or spinal complexity than those previously identified (Briona et al., 2015; Wehner et al., 2018).

Lastly, whether axons require a glial bridge to cross the site of injury is still controversial (Cigliola et al., 2020). Axons severed during injury from neurons with cell bodies located in the brain, regrow and innervate their target to restore function (Becker et al., 1997); however, axonal regeneration is slowed in aging zebrafish (Graciarena et al., 2014). Ablation of Gfap+ cells with nitroreductase demonstrated that axons could cross the injury site in the absence of a glial bridge (Wehner et al., 2018) suggesting a glial bridge is not necessary for axonal regrowth. We used live imaging to look at the timing of axonal growth and glial bridge formation (Fig. 4). In line with previous studies, axons were able to cross the site of injury before the glial bridge formed for all three ages. Strikingly, we found a larger of percentage of zebrafish had axons cross the site of injury suggesting that the glia bridge does not dictate whether axons can cross the site of injury. In adult zebrafish, bridging glial were transcriptionally similar to scar-bordering astrocytes found in mammals (Klatt Shaw et al., 2021) suggesting that the accumulation of signal observed may correlate with reactive gliosis. Therefore, studies looking at interactions between radial glia and axons at the injury border could shed light on whether the glial environment, metabolic state of radial glia, or other intrinsic properties dictates whether axons can cross the site of injury (Li et al., 2020a). Future studies combining transgenic lines with more efficient (Labbaf et al., 2022) and/or spatiotemporally controlled ablation (Mruk et al., 2020) could provide further insights into the axonal-glial interactions that occur during regrowth.

Given that the number of laboratories studying SCI in zebrafish is steadily increasing, the need to standardize and expand these studies to include additional physiological considerations is vital for understanding the mechanisms of regeneration.

METHODS

Zebrafish husbandry

Adult zebrafish [wild-type AB and *Tg(gfap:EGFP)*], 3-18 months, were a generous gift from the Chen Lab (Stanford). *Tg(olig2:dsRed)* were a generous gift from the Appel lab (UC Anschutz) (Kucenas et al., 2008). All zebrafish larvae were raised on a rotifer/brine shrimp diet starting at 5 days post fertilization (dpf) unless otherwise indicated. Adults were maintained at 28.5°C on a 14:10 hour light:dark cycle and fed in the morning with Ziegler's adult zebrafish diet and in the afternoon with brine shrimp. Embryos were staged as described previously (Kimmel et al., 1995). Embryos were obtained through natural matings and cultured at 28–30°C in E3 medium. To prevent pigmentation for fluorescence, immunohistochemistry, and *in situ* imaging, the culture medium was also supplemented with 0.003% (w/v) N-phenylthiourea (PTU, Sigma-Aldrich #P7629). The IACUC committee at the University of Wyoming approved all animal procedures.

Line Generation

The generation of the Tol2-*elavl3:mCherry-CAAX* plasmid is previously described (Mruk et al., 2020). Transgenic zebrafish were generated using Tol2-mediated transgenesis (Abe et al., 2011; Suster et al., 2009). Plasmid DNA and Tol2 mRNA were premixed and co-injected into one-cell-stage embryos (50 pg of plasmid; 50 pg of mRNA). Fish were raised to adulthood and mated with wild-type AB fish to identify founders with germline transmission, and those yielding F2 generations with monoallelic expression were used to establish the *Tg(elavl3:mCherry-CAAX*) transgenic line. The Tol2-*elavl3:mCherry-CAAX* plasmid and line are available upon request.

Zebrafish transection

Larval zebrafish at 3, 5, or 7 dpf were mounted on flat slides in 2% low melting-point (LMP) agarose and briefly anesthetized using 0.01% tricaine (Western Chemical). The spinal cord was transected with a microblade (WPI#501731 or WPI#500249) at the level of the cloaca. Larvae were allowed to recover for approximately 2 hours in petri dishes filled with E2 buffer supplemented with penicillin/streptomycin (Pen/Strep, 100 unit, 100 ug/mL, Gibco #15140-122), before mounting and imaging (Briona and Dorsky, 2014b). Larvae used for fluorescent imaging were also supplemented with 0.003% PTU. For multi-day experiments, E2 buffer was replaced daily. Larvae were not fed on the day of transection.

Survival

Tg(gfap:EGFP) larvae were transected as described at 3, 5, or 7 dpf. Transected and age-matched control larvae were maintained as described in petri dishes filled with E2 buffer. Larvae were counted daily from 1 dpi to 7 dpi. Decreases in total dish population were recorded as deaths. Surviving larvae were censored at the end of the observation period. A logrank Mantel-Cox test was used to determine whether the survival curves of transected fish differed from those of their age matched control larvae. A $p < 0.05$ was considered significant. Survival of each age of transection and their age matched controls were graphed as a Kaplan Meier curves.

Heartrate quantification

Live larvae were mounted were mounted in 1.5% LMP agarose on a glass slide and heartbeat was recorded via Olympus SZX16 stereoscope with an Olympus DP80 camera and SDF PLANO 1XPF objective based on ZebraPace (Gaur et al., 2018). Thirty second uncompressed AVI format videos

were taken using Olympus cellSens software. Files were opened in FIJI software in grayscale mode without a virtual stack (Schindelin et al., 2012). A circular region of interest (ROI) was drawn on the AVI video file on the edge of the cardiac ventricle of the zebrafish larvae. Using ImageJ's "plot-z-axis profile," a time profile was generated via the pixel intensity change of the ROI. Peak detection and heartbeat counting was performed in MS Excel as previously described (Gaur et al., 2018). For each video, three 10-second sections were sampled and averaged to mediate random error. All videos were analyzed by a student blinded to the experimental conditions.

Swim bladder inflation

Transgenic larvae from both *Tg(gfap:EGFP)* and *Tg(olig2:dsRed)* were transected as described. Larvae were observed each day, counting the number of animals with an inflated swim bladder each morning. Representative larvae from each condition were mounted in 1% LMP agarose and imaged on the Olympus SZX16 stereoscope with an Olympus DP80 camera and SDF PLANO 1XPF objective. Images were taken using the Olympus cellSens software.

Fluorescence intensity quantification

Live larvae were mounted in 1.5% LMP agarose on a glass slide. Larvae were imaged using a Leica DM6B epifluorescence microscope with Leica DFC 900 GT camera, CoolLED pE-300 Ultra light source, 2.5x/NA 0.07 objective and 20x/NA 0.5 water immersion objective. Bright field and green fluorescent images were taken for both 2.5x and 20x images. Images taken at 20x used z-stack with a constant system optimized step size of 2.05 micron using Leica Application Suite X. Images were processed in Leica Application Suite X with Leica Thunder Instant Computational Clearing using the pre-installed water correction factor. To quantify pixel intensity, raw green,

fluorescent 20x z-stacks were opened in FIJI as maximum projections. The region of interest was selected using the segmented line selection tool at 100-point width. The Plot Profile analysis tool was then used to measure pixel intensity across the region of interest. Larvae with injuries larger than 250 micron, and larvae that did not survive the entire study were excluded from analysis.

Confocal Imaging for Glial & Axonal Bridging

Heterozygous *Tg(elavl3:mCherry-CAAX)* larvae were crossed with *Tg(gfap:EGFP)* larvae to generate *Tg(elavl3:mCherry-CAAX; gfap:EGFP)* larvae. Larvae were transected as described above. Both transected and uncut controls were mounted in 1% LMP agarose and imaged on a Zeiss LSM 700 confocal microscope equipped with a 20x/NA 0.5 water-immersion objective. Z-stacks were generated from images taken at 2-5 µm intervals using the following settings: 2048x2048 pixels, 8 speed, 4 averaging. Maximum intensity projections were made in ImageJ and bridging was determined by observation of a complete track of fluorescence across the site of injury. Larvae that did not survive the entire study were excluded from analysis.

In situ hybridization

Whole-mount *in situ* hybridization was done using standard protocols with some modifications (Broadbent and Read, 1999). Zebrafish cDNA was prepared from RNA extracted from AB zebrafish (1–7 dpf) using Trizol (Ambion #15596026) and phenol:chloroform (Millipore #19K0856166). cDNA was generated using the SuperScript IV reverse transcriptase system (Invitrogen #18091150) using dT primers to target mRNA. T3-promoter containing PCR products were then amplified with the designated primers (T3 sequence underlined): *ctgfa:* 5′-tgtgattgctctgctgttcc-3′, and 5′-<u>aattaaccctcactaaagggg</u>tgaggcgattagcttctg-3′ (Mokalled et al., 2016).

RNA probes were *in vitro* transcribed from the PCR products using the MEGAscript T3 Transcription Kit (Invitrogen #AM1338), substituting nucleotides from the kit with digoxigenin-UTP (Roche #11277073910). After injury, embryos were fixed at the desired timepoint in 4% (w/v) paraformaldehyde (PFA) in PBS at 4°C overnight and then stored in methanol. After rehydration, embryos were permeabilized with proteinase K (Roche #03115887001). Proteinase K treatment was adjusted based on age (Table 2) and samples refixed in 4% PFA in PBS for 60 mins. Sheep anti-digoxigenin-AP antibody (Roche #11093274910) was used at 1:500 concentration as previously reported (Mruk et al., 2020). All samples were cleared using 0.5 M glycine and ethanol, and imaged on an Olympus SZX16 stereoscope with an Olympus DP80 camera and SDF PLANO 1XPF objective. Images were captured using cellSens software.

Acridine orange staining and cell counting

Tg(olig2:dsRed) embryos were transected as described. Live transected larvae were soaked in 5 µg/mL of acridine orange in E2 buffer in the dark for 1 hour at 28-29°C. Embryos were then washed 3 times for 5 minutes each in fresh E2 buffer, mounted on glass slides in 1% LMP agarose, and imaged on a Leica DM6D epifluorescence microscope with a Leica DFC900GT camera and CoolLED pE-300 Ultra light source or on a Zeiss LSM 700 confocal microscope equipped with a MA-PMT with 20x/NA 0.5 water immersion objective. Z-stacks were generated from images taken at 2-5 µm intervals using the following settings: 1024x1024 pixels, 9 speed, 4 averaging. Cells were counted by two individual researchers and the average of the two researchers for each larvae plotted.

Quantitative PCR

Tg(gfap:EGFP) larvae were transected as described. Five larvae for each condition for each time point were selected and cDNA generated as described above. cDNA samples were cleaned using ethanol precipitation. Approximately 200 ng of each cDNA sample was used as templates for qPCR using the Maxima SYBR Green/ROX master mix (Thermo Scientific #K0221). Target sequences for qPCR were amplified using the following primers: *gfap*: 5'-TAAGCCAGACTTGACCGCTG-3' and 5'-TTACGATTGGCTGCATCCGT-3', *ctgfa*: 5'-TGACTACGGCTCCCCAAGTA-3' and 5'-TCCACTGCGGTACACCATTC-3'. The internal control was *gapdh*, using the following primers: 5'-GTGGAGTCTACTGGTGTCTTC-3' and 5'-GTGCAGGAGGCATTGCTTACA-3' (DiMuccio et al., 2005). Relative mRNA levels were determined using the $\Delta\Delta C_t$ method. The relative fold change was calculated using $2^{-\Delta\Delta Ct}$.

Locomotion behavior

Tg(gfap:EGFP) larvae were transected as described and locomotion recorded through 12 dpf. Larval zebrafish reliably show activity on transition to a dark environment from a lit environment and are more active in the morning beginning around 10 am and reach their lowest activity in the evening by 5 pm (MacPhail et al., 2009). Behavior experiments were conducted between 2:30-3:30 pm for 5 dpf larvae and 10:00-11:00 am for 7 dpf larvae. A clear 48-well plate was used with one larvae per well in a fixed volume of 1 mL of E2 supplemented with Pen/Strep. Locomotion was assessed using a Zebrabox and its ViewPoint LS tracking software (Viewpoint Life Sciences, Lyon, France). Larvae were acclimated to the test environment for 10 minutes, followed by a 10-minute session in a dark environment. Locomotion speed from various movement types (twitch: 0-2 mm/s; small: 2-4 mm/s; large: >4 mm/s) was video recorded. Following behavior experiments,

larvae were imaged and scored by an independent experimenter using an Olympus SZX16 stereoscope with an Olympus DP80 camera and SDF PLANO 1XPF objective. cellSens software was used to capture images. Larvae that did not survive the entire study were excluded from analysis.

Statistics

For all zebrafish experiments, at least two breeding tanks, each containing 2 to 4 males and 2 to 4 females from separate stocks, were set up to generate embryos. Embryos from each tank were randomly distributed across tested conditions, and unfertilized and developmentally abnormal embryos were removed prior to transection or compound treatment. Samples sizes were calculated for a 30% effect with 80% power. For all graphs, values for individual fish are plotted, and data is presented as the mean ± standard deviation (SD). For statistical testing, each distribution was assessed using the Shapiro-Wilk test and determined to be non-normal. Significant differences were determined using either an unpaired Mann-Whitney t-test or a Kruskal-Wallis ANOVA test with a post hoc Dunn's test. P values of < 0.05 were considered statistically significant. Graphs were generated using GraphPad Prism 9 (Dotmatics) software. Additional experimental statistics for the phenotypic distributions are reported in Tables S1-S4.

ACKNOWLEDGMENTS

We gratefully acknowledge financial support from NIH P20 GM121310 (K.M.) and the McNair Scholars program (S.L). Confocal imaging was supported in part by the University of Wyoming's Integrated Microscopy Core (NIH P20GM121310).

AUTHOR CONTRIBUTIONS

Conceptualization: K.M.; Methodology: K.L.U., W.J.W., P.I.G., S.L., K.M.; Validation: K.L.U., W.J.W., P.I.G., K.M.; Formal analysis: K.L.U., W.J.W., P.I.G., S.L., T.P.R., K.M.; Investigation: K.L.U., W.J.W., P.I.G., K.M.; Resources: W.J.W., T.P.R. Writing: K.L.U, W.J.W, P.I.G., S.L., K.M.; Writing - review & editing: K.L.U., W.J.W., P.I.G., T.P.R., K.M.; Visualization: K.L.U., W.J.W., P.I.G., K.M. Supervision: K.M.; Project administration: K.M.; Funding acquisition: K.M.

COMPETING FINANCIAL INTERESTS

The authors declare no competing financial interests

SUPPORTING INFORMATION

Tables S1-S3

Figs. S1-S3

TABLES

Table 1. Relative fold changes of gfap and ctgfa after injury.[a]

Gene	Days post injury (dpi)	3 dpf SCI	5 dpf SCI	7 dpf SCI
gfap	1 dpi	0.65 ± 0.27	0.20 ± 0.70	1.8 ± 0.55
gfap	2 dpi	0.47 ± 0.93	0.57 ± 0.33	0.89 ± 0.70
gfap	3 dpi	0.75 ± 0.97	0.96 ± 1.02	1.5 ± 0.21
gfap	4 dpi	3.0 ± 0.80	1.4 ± 0.72	1.0 ± 0.42
gfap	5 dpi	0.47 ± 0.78	1.0 ± 0.56	1.2 ± 0.60
ctgfa	1 dpi	0.15 ± 0.68	0.21 ± 2.05	0.65 ± 0.87
ctgfa	2 dpi	0.34 ± 1.5	1.1 ± 0.67	0.86 ± 1.72
ctgfa	3 dpi	0.59 ± 0.65	2.5 ± 0.61	2.8 ± 0.62
ctgfa	4 dpi	348 ± 5.2	4.3 ± 0.38	4.0 ± 0.66
ctgfa	5 dpi	0.67 ± 1.1	2.4 ± 0.55	6.9 ± 0.92

[a]Fold changes are presented as mean ± SEM.

Table 2. Proteinase K concentrations used based on age of larvae

Larval Age (dpf)	Proteinase K Concentration (µg/mL)	Time of Treatment (min)
3	5	60
4	5	90
5, 6	15	30
7	15	60
8, 9	15	90
10, 11, 12	15	120

FIGURE LEGENDS

Fig. 1. Survival and amount of cell death varies with age of transection. Survival was measured after SCI for larvae transected at (**A**) 3 dpf, (**B**) 5 dpf, and (**C**) 7 dpf. Graphs are Kaplan-Meier curves for control (black) and SCI (red). The survival curves for larvae transected at 3 dpf and 5 dpf differed significantly from controls (χ^2=20.46, p<0.0001 and χ^2=16.69, p<0.0001 respectively). The survival curves for larvae transected at 7 dpf, did not differ significantly (χ^2=0.6671, p = 0.7962) between control and SCI. Statistics for the observed phenotypes are in Table S1. (**D**) Representative micrographs from *Tg(olig2:dsRed)* larvae incubated in acridine orange 24 hours post injury (hpi) are shown, with green signal indicating cell death. Positive cells (white arrowheads) were counted in the region of the spinal cord, determined by dsRed signal. Larvae orientation: lateral view, anterior left. (**E**) Quantification of apoptotic cells. The number of cells in individual fish are plotted as the average from two independent counters. Mean ± standard deviation is shown. Scale bar = 50 µm. Statistics for the observed phenotypes are in Table S2.

Figure 2. Transected larvae form a radial glia bridge and upregulate *ctgfa* expression by 3 dpi. (**A**) *Tg(gfap:EGFP)* larvae were transected at 5 dpf and followed individually for 5 days post injury (dpi). Bright field and fluorescent micrographs from a single reprensetative larvae are

shown. Scale bar: 500 µm. Inset: Maximum intensity projection processed with Leica Thunder Instant Computational Clearing. Scale bar: 100 µm. Larvae orientation: lateral view, anterior left. (**B**). Quantification of pixel intensity. Mean pixel intensity (solid line) and standard deviation (shading) for control (black) and transected (red) larvae are graphed approximately every 10 µm for clarity. Epicenter of the lesion denoted as 0 on the X-axis was determined by the lowest average normalized pixel intensity value on day of injury (0 dpi). Pixel intensity increases proximal to the lesion and persists through bridge formation indicating a local increase GFP signal. (**C**) *ctgfa* expression (blue staining) was determined after SCI at 3 dpf, 5 dpf (**D**), and 7 dpf (**E**). Increased expression in the spinal cord is limited to site of injury through 5 dpi. Representative brightfield micrographs are shown. Larvae orientation: lateral view, anterior left. Scale bars: 500 µm and 100 µm. Statistics for the observed phenotypes are in Table S3.

Figure 3. Transected larvae recover swim behavior in a glial-bridge dependent manner. *Tg(gfap:EGFP)* larvae were transected at 5 dpf and free swim followed individually. **(A)** Average swim distances (mm) of control vs transected larvae generated from different swim speeds. Top panel: twitch movement (<2 mm/s), middle panel: small movement (2-4 mm/s), bottom panel: large movement (>4 mm/s). Distance was quantified by averaging five 2-min bins. Mean ± SD are shown with individual larvae plotted. The nonparametric Mann-Whitney test was used to determine significance. Control: n=27, SCI: n= 21 (**B**) Average swim distances from different swim speeds plotted as a function of glial bridge formation. An experimenter blinded to the swim data imaged larvae for the presence of a bridge. The nonparametric Kruskal-Wallis test was used to determine significance and adjusted p values are reported. Control: n=27; Bridged: n=14; No bridge: n=6.

Figure 4: Some axons cross the site of injury independent of glial bridge formation. (**A**) *Tg(elavl3:mCherry-CAAX; gfap:EGFP)* larvae were transected and imaged each day through 5 days post injury (dpi). Representative micrographs from a maximal intensity projection of the spinal cord. A single larvae was tracked to show day of injury (0 dpi) and end of experiment (5 dpi). Larvae orientation: lateral view, anterior left. Scale bar: 50 µm. (**B**) Quantification of bridging results. Percentage of animals that formed a glial and/or axonal bridge are shown. For all ages, axon bridging percentage was higher than that of glial bridging. Bridging was determined by complete tracks of fluorescence across the site of injury. 3 dpf: control: n = 24, SCI: n = 18; 5 dpf: control: n=26, SCI: n = 20; 7 dpf: control: n=21, SCI: n = 17 SCI, all tracked individually. Statistics for the observed phenotypes are in Table S4.

REFERENCES

Abe, G., Suster, M.L., Kawakami, K., 2011. Tol2-mediated transgenesis, gene trapping, enhancer trapping, and the Gal4-UAS system. Methods in cell biology 104, 23-49.

Alper, S.R., Dorsky, R.I., 2022. Unique advantages of zebrafish larvae as a model for spinal cord regeneration. Frontiers in molecular neuroscience 15, 983336.

Anguita-Salinas, C., Sánchez, M., Morales, R.A., Ceci, M.L., Rojas-Benítez, D., Allende, M.L., 2019. Cellular Dynamics during Spinal Cord Regeneration in Larval Zebrafish. Developmental neuroscience 41, 112-122.

Becker, T., Wullimann, M.F., Becker, C.G., Bernhardt, R.R., Schachner, M., 1997. Axonal regrowth after spinal cord transection in adult zebrafish. The Journal of comparative neurology 377, 577-595.

Bensimon-Brito, A., Cardeira, J., Cancela, M.L., Huysseune, A., Witten, P.E., 2012. Distinct patterns of notochord mineralization in zebrafish coincide with the localization of Osteocalcin isoform 1 during early vertebral centra formation. BMC developmental biology 12, 28.

Berg, E.M., Mrowka, L., Bertuzzi, M., Madrid, D., Picton, L.D., El Manira, A., 2023. Brainstem circuits encoding start, speed, and duration of swimming in adult zebrafish. Neuron 111, 372-386 e374.

Bhatt, D.H., Otto, S.J., Depoister, B., Fetcho, J.R., 2004. Cyclic AMP-induced repair of zebrafish spinal circuits. Science (New York, N.Y.) 305, 254-258.

Bin, J.M., Lyons, D.A., 2016. Imaging Myelination In Vivo Using Transparent Animal Models. Brain plasticity (Amsterdam, Netherlands) 2, 3-29.

Briona, L.K., Dorsky, R.I., 2014a. Radial glial progenitors repair the zebrafish spinal cord following transection. Experimental neurology 256, 81-92.

Briona, L.K., Dorsky, R.I., 2014b. Spinal cord transection in the larval zebrafish. Journal of visualized experiments : JoVE.

Briona, L.K., Poulain, F.E., Mosimann, C., Dorsky, R.I., 2015. Wnt/ß-catenin signaling is required for radial glial neurogenesis following spinal cord injury. Developmental biology 403, 15-21.

Broadbent, J., Read, E.M., 1999. Wholemount in situ hybridization of Xenopus and zebrafish embryos. Methods in molecular biology (Clifton, N.J.) 127, 57-67.

Brösamle, C., Halpern, M.E., 2002. Characterization of myelination in the developing zebrafish. Glia 39, 47-57.

Brown, D.R., Samsa, L.A., Qian, L., Liu, J., 2016. Advances in the Study of Heart Development and Disease Using Zebrafish. Journal of cardiovascular development and disease 3.

Brustein, E., Saint-Amant, L., Buss, R.R., Chong, M., McDearmid, J.R., Drapeau, P., 2003. Steps during the development of the zebrafish locomotor network. Journal of physiology, Paris 97, 77-86.

Cavone, L., McCann, T., Drake, L.K., Aguzzi, E.A., Oprişoreanu, A.M., Pedersen, E., Sandi, S., Selvarajah, J., Tsarouchas, T.M., Wehner, D., Keatinge, M., Mysiak, K.S., Henderson, B.E.P., Dobie, R., Henderson, N.C., Becker, T., Becker, C.G., 2021. A unique macrophage subpopulation signals directly to progenitor cells to promote regenerative neurogenesis in the zebrafish spinal cord. Developmental cell 56, 1617-1630 e1616.

Cigliola, V., Becker, C.J., Poss, K.D., 2020. Building bridges, not walls: spinal cord regeneration in zebrafish. Disease models & mechanisms 13.

DiMuccio, T., Mukai, S.T., Clelland, E., Kohli, G., Cuartero, M., Wu, T., Peng, C., 2005. Cloning of a second form of activin-betaA cDNA and regulation of activin-betaA subunits and activin type

II receptor mRNA expression by gonadotropin in the zebrafish ovary. General and comparative endocrinology 143, 287-299.

Drake, L.K., Keatinge, M., Tsarouchas, T.M., Becker, C.G., Lyons, D.A., Becker, T., 2023. Rapid Testing of Gene Function in Axonal Regeneration After Spinal Cord Injury Using Larval Zebrafish. Methods in molecular biology (Clifton, N.J.) 2636, 263-277.

Drapeau, P., Saint-Amant, L., Buss, R.R., Chong, M., McDearmid, J.R., Brustein, E., 2002. Development of the locomotor network in zebrafish. Progress in neurobiology 68, 85-111.

Fang, P., Lin, J.F., Pan, H.C., Shen, Y.Q., Schachner, M., 2012. A surgery protocol for adult zebrafish spinal cord injury. Journal of genetics and genomics = Yi chuan xue bao 39, 481-487.

Fang, P., Pan, H.C., Lin, S.L., Zhang, W.Q., Rauvala, H., Schachner, M., Shen, Y.Q., 2014. HMGB1 contributes to regeneration after spinal cord injury in adult zebrafish. Molecular neurobiology 49, 472-483.

Flores, E.M., Nguyen, A.T., Odem, M.A., Eisenhoffer, G.T., Krachler, A.M., 2020. The zebrafish as a model for gastrointestinal tract-microbe interactions. Cellular microbiology 22, e13152.

Garcia, A.L., Udeh, A., Kalahasty, K., Hackam, A.S., 2018. A growing field: The regulation of axonal regeneration by Wnt signaling. Neural regeneration research 13, 43-52.

Gaur, H., Pullaguri, N., Nema, S., Purushothaman, S., Bhargava, Y., Bhargava, A., 2018. ZebraPace: An Open-Source Method for Cardiac-Rhythm Estimation in Untethered Zebrafish Larvae. Zebrafish 15, 254-262.

Ghosh, S., Hui, S.P., 2018. Axonal regeneration in zebrafish spinal cord. Regeneration (Oxford, England) 5, 43-60.

Goldshmit, Y., Sztal, T.E., Jusuf, P.R., Hall, T.E., Nguyen-Chi, M., Currie, P.D., 2012. Fgf-dependent glial cell bridges facilitate spinal cord regeneration in zebrafish. The Journal of neuroscience : the official journal of the Society for Neuroscience 32, 7477-7492.

Gollmann-Tepeköylü, C., Nägele, F., Graber, M., Pölzl, L., Lobenwein, D., Hirsch, J., An, A., Irschick, R., Röhrs, B., Kremser, C., Hackl, H., Huber, R., Venezia, S., Hercher, D., Fritsch, H., Bonaros, N., Stefanova, N., Tancevski, I., Meyer, D., Grimm, M., Holfeld, J., 2020. Shock waves promote spinal cord repair via TLR3. JCI insight 5.

Graciarena, M., Dambly-Chaudière, C., Ghysen, A., 2014. Dynamics of axonal regeneration in adult and aging zebrafish reveal the promoting effect of a first lesion. Proceedings of the National Academy of Sciences of the United States of America 111, 1610-1615.

Grigorean, V.T., Sandu, A.M., Popescu, M., Iacobini, M.A., Stoian, R., Neascu, C., Strambu, V., Popa, F., 2009. Cardiac dysfunctions following spinal cord injury. Journal of medicine and life 2, 133-145.

Hernandez, R.E., Galitan, L., Cameron, J., Goodwin, N., Ramakrishnan, L., 2018. Delay of Initial Feeding of Zebrafish Larvae Until 8 Days Postfertilization Has No Impact on Survival or Growth Through the Juvenile Stage. Zebrafish 15, 515-518.

Hossainian, D., Shao, E., Jiao, B., Ilin, V.A., Parris, R.S., Zhou, Y., Bai, Q., Burton, E.A., 2022. Quantification of functional recovery in a larval zebrafish model of spinal cord injury. Journal of neuroscience research 100, 2044-2054.

Huang, C.X., Wang, Z., Cheng, J., Zhu, Z., Guan, N.N., Song, J., 2022. De novo establishment of circuit modules restores locomotion after spinal cord injury in adult zebrafish. Cell reports 41, 111535.

Huang, C.X., Zhao, Y., Mao, J., Wang, Z., Xu, L., Cheng, J., Guan, N.N., Song, J., 2021. An injury-induced serotonergic neuron subpopulation contributes to axon regrowth and function restoration after spinal cord injury in zebrafish. Nature communications 12, 7093.

Hui, S.P., Dutta, A., Ghosh, S., 2010. Cellular response after crush injury in adult zebrafish spinal cord. Developmental dynamics : an official publication of the American Association of Anatomists 239, 2962-2979.

Hui, S.P., Sengupta, D., Lee, S.G., Sen, T., Kundu, S., Mathavan, S., Ghosh, S., 2014. Genome wide expression profiling during spinal cord regeneration identifies comprehensive cellular responses in zebrafish. PloS one 9, e84212.

John, N., Kolb, J., Wehner, D., 2022. Mechanical spinal cord transection in larval zebrafish and subsequent whole-mount histological processing. STAR protocols 3, 101093.

Keatinge, M., Tsarouchas, T.M., Munir, T., Porter, N.J., Larraz, J., Gianni, D., Tsai, H.H., Becker, C.G., Lyons, D.A., Becker, T., 2021. CRISPR gRNA phenotypic screening in zebrafish reveals pro-regenerative genes in spinal cord injury. PLoS genetics 17, e1009515.

Kim, H., Kim, S., Chung, A.Y., Bae, Y.K., Hibi, M., Lim, C.S., Park, H.C., 2008. Notch-regulated perineurium development from zebrafish spinal cord. Neuroscience letters 448, 240-244.

Kimmel, C.B., Ballard, W.W., Kimmel, S.R., Ullmann, B., Schilling, T.F., 1995. Stages of embryonic development of the zebrafish. Developmental dynamics : an official publication of the American Association of Anatomists 203, 253-310.

Kirby, B.B., Takada, N., Latimer, A.J., Shin, J., Carney, T.J., Kelsh, R.N., Appel, B., 2006. In vivo time-lapse imaging shows dynamic oligodendrocyte progenitor behavior during zebrafish development. Nature neuroscience 9, 1506-1511.

Kishore, S., Bagnall, M.W., McLean, D.L., 2014. Systematic shifts in the balance of excitation and inhibition coordinate the activity of axial motor pools at different speeds of locomotion. The Journal of neuroscience : the official journal of the Society for Neuroscience 34, 14046-14054.

Klatt Shaw, D., Saraswathy, V.M., Zhou, L., McAdow, A.R., Burris, B., Butka, E., Morris, S.A., Dietmann, S., Mokalled, M.H., 2021. Localized EMT reprograms glial progenitors to promote spinal cord repair. Developmental cell 56, 613-626 e617.

Kolvenbach, C.M., Dworschak, G.C., Rieke, J.M., Woolf, A.S., Reutter, H., Odermatt, B., Hilger, A.C., 2023. Modelling human lower urinary tract malformations in zebrafish. Molecular and cellular pediatrics 10, 2.

Kucenas, S., Takada, N., Park, H.C., Woodruff, E., Broadie, K., Appel, B., 2008. CNS-derived glia ensheath peripheral nerves and mediate motor root development. Nature neuroscience 11, 143-151.

Labbaf, Z., Petratou, K., Ermlich, L., Backer, W., Tarbashevich, K., Reichman-Fried, M., Luschnig, S., Schulte-Merker, S., Raz, E., 2022. A robust and tunable system for targeted cell ablation in developing embryos. Developmental cell 57, 2026-2040 e2025.

Li, F., Sami, A., Noristani, H.N., Slattery, K., Qiu, J., Groves, T., Wang, S., Veerasammy, K., Chen, Y.X., Morales, J., Haynes, P., Sehgal, A., He, Y., Li, S., Song, Y., 2020a. Glial Metabolic Rewiring Promotes Axon Regeneration and Functional Recovery in the Central Nervous System. Cell metabolism 32, 767-785 e767.

Li, J.H., Shi, Z.J., Li, Y., Pan, B., Yuan, S.Y., Shi, L.L., Hao, Y., Cao, F.J., Feng, S.Q., 2020b. Bioinformatic identification of key candidate genes and pathways in axon regeneration after spinal cord injury in zebrafish. Neural regeneration research 15, 103-111.

MacPhail, R.C., Brooks, J., Hunter, D.L., Padnos, B., Irons, T.D., Padilla, S., 2009. Locomotion in larval zebrafish: Influence of time of day, lighting and ethanol. Neurotoxicology 30, 52-58.

Matsuoka, R.L., Marass, M., Avdesh, A., Helker, C.S., Maischein, H.M., Grosse, A.S., Kaur, H., Lawson, N.D., Herzog, W., Stainier, D.Y., 2016. Radial glia regulate vascular patterning around the developing spinal cord. eLife 5.

Mizuno, Y., Mochizuki, H., Sugita, Y., Goto, K., 1998. Apoptosis in neurodegenerative disorders. Internal medicine (Tokyo, Japan) 37, 192-193.

Mokalled, M.H., Patra, C., Dickson, A.L., Endo, T., Stainier, D.Y., Poss, K.D., 2016. Injury-induced ctgfa directs glial bridging and spinal cord regeneration in zebrafish. Science (New York, N.Y.) 354, 630-634.

Mruk, K., Ciepla, P., Piza, P.A., Alnaqib, M.A., Chen, J.K., 2020. Targeted cell ablation in zebrafish using optogenetic transcriptional control. Development (Cambridge, England) 147.

Noorimotlagh, Z., Babaie, M., Safdarian, M., Ghadiri, T., Rahimi-Movaghar, V., 2017. Mechanisms of spinal cord injury regeneration in zebrafish: a systematic review. Iranian journal of basic medical sciences 20, 1287-1296.

Ohnmacht, J., Yang, Y., Maurer, G.W., Barreiro-Iglesias, A., Tsarouchas, T.M., Wehner, D., Sieger, D., Becker, C.G., Becker, T., 2016. Spinal motor neurons are regenerated after mechanical lesion and genetic ablation in larval zebrafish. Development (Cambridge, England) 143, 1464-1474.

Outtandy, P., Russell, C., Kleta, R., Bockenhauer, D., 2019. Zebrafish as a model for kidney function and disease. Pediatric nephrology (Berlin, Germany) 34, 751-762.

Panula, P., Sallinen, V., Sundvik, M., Kolehmainen, J., Torkko, V., Tiittula, A., Moshnyakov, M., Podlasz, P., 2006. Modulatory neurotransmitter systems and behavior: towards zebrafish models of neurodegenerative diseases. Zebrafish 3, 235-247.

Parichy, D.M., Elizondo, M.R., Mills, M.G., Gordon, T.N., Engeszer, R.E., 2009. Normal table of postembryonic zebrafish development: staging by externally visible anatomy of the living fish. Developmental dynamics : an official publication of the American Association of Anatomists 238, 2975-3015.

Park, H.C., Mehta, A., Richardson, J.S., Appel, B., 2002. olig2 is required for zebrafish primary motor neuron and oligodendrocyte development. Developmental biology 248, 356-368.

Partida, E., Mironets, E., Hou, S., Tom, V.J., 2016. Cardiovascular dysfunction following spinal cord injury. Neural regeneration research 11, 189-194.

Popa, C., Popa, F., Grigorean, V.T., Onose, G., Sandu, A.M., Popescu, M., Burnei, G., Strambu, V., Sinescu, C., 2010. Vascular dysfunctions following spinal cord injury. Journal of medicine and life 3, 275-285.

Preston, M.A., Macklin, W.B., 2015. Zebrafish as a model to investigate CNS myelination. Glia 63, 177-193.

Reimer, M.M., Kuscha, V., Wyatt, C., Sörensen, I., Frank, R.E., Knüwer, M., Becker, T., Becker, C.G., 2009. Sonic hedgehog is a polarized signal for motor neuron regeneration in adult zebrafish. The Journal of neuroscience : the official journal of the Society for Neuroscience 29, 15073-15082.

Reimer, M.M., Norris, A., Ohnmacht, J., Patani, R., Zhong, Z., Dias, T.B., Kuscha, V., Scott, A.L., Chen, Y.C., Rozov, S., Frazer, S.L., Wyatt, C., Higashijima, S., Patton, E.E., Panula, P., Chandran, S., Becker, T., Becker, C.G., 2013. Dopamine from the brain promotes spinal motor neuron generation during development and adult regeneration. Developmental cell 25, 478-491.

Sadler, K.C., Rawls, J.F., Farber, S.A., 2013. Getting the inside tract: new frontiers in zebrafish digestive system biology. Zebrafish 10, 129-131.

Schindelin, J., Arganda-Carreras, I., Frise, E., Kaynig, V., Longair, M., Pietzsch, T., Preibisch, S., Rueden, C., Saalfeld, S., Schmid, B., Tinevez, J.Y., White, D.J., Hartenstein, V., Eliceiri, K., Tomancak, P., Cardona, A., 2012. Fiji: an open-source platform for biological-image analysis. Nature methods 9, 676-682.

Severi, K.E., Portugues, R., Marques, J.C., O'Malley, D.M., Orger, M.B., Engert, F., 2014. Neural control and modulation of swimming speed in the larval zebrafish. Neuron 83, 692-707.

Suster, M.L., Kikuta, H., Urasaki, A., Asakawa, K., Kawakami, K., 2009. Transgenesis in zebrafish with the tol2 transposon system. Methods in molecular biology (Clifton, N.J.) 561, 41-63.

Tsarouchas, T.M., Wehner, D., Cavone, L., Munir, T., Keatinge, M., Lambertus, M., Underhill, A., Barrett, T., Kassapis, E., Ogryzko, N., Feng, Y., van Ham, T.J., Becker, T., Becker, C.G., 2018. Dynamic control of proinflammatory cytokines Il-1β and Tnf-α by macrophages in zebrafish spinal cord regeneration. Nature communications 9, 4670.

Vajn, K., Suler, D., Plunkett, J.A., Oudega, M., 2014. Temporal profile of endogenous anatomical repair and functional recovery following spinal cord injury in adult zebrafish. PloS one 9, e105857.

van Raamsdonk, W., Smit-Onel, M.J., Maslam, S., Velzing, E., de Heus, R., 1998. Changes in the synaptology of spinal motoneurons in zebrafish following spinal cord transection. Acta histochemica 100, 133-148.

Vandestadt, C., Vanwalleghem, G.C., Khabooshan, M.A., Douek, A.M., Castillo, H.A., Li, M., Schulze, K., Don, E., Stamatis, S.A., Ratnadiwakara, M., Änkö, M.L., Scott, E.K., Kaslin, J., 2021.

RNA-induced inflammation and migration of precursor neurons initiates neuronal circuit regeneration in zebrafish. Developmental cell 56, 2364-2380 e2368.

Wehner, D., Becker, T., Becker, C.G., 2018. Restoration of anatomical continuity after spinal cord transection depends on Wnt/β-catenin signaling in larval zebrafish. Data in brief 16, 65-70.

Winata, C.L., Korzh, S., Kondrychyn, I., Zheng, W., Korzh, V., Gong, Z., 2009. Development of zebrafish swimbladder: The requirement of Hedgehog signaling in specification and organization of the three tissue layers. Developmental biology 331, 222-236.

Figure 1

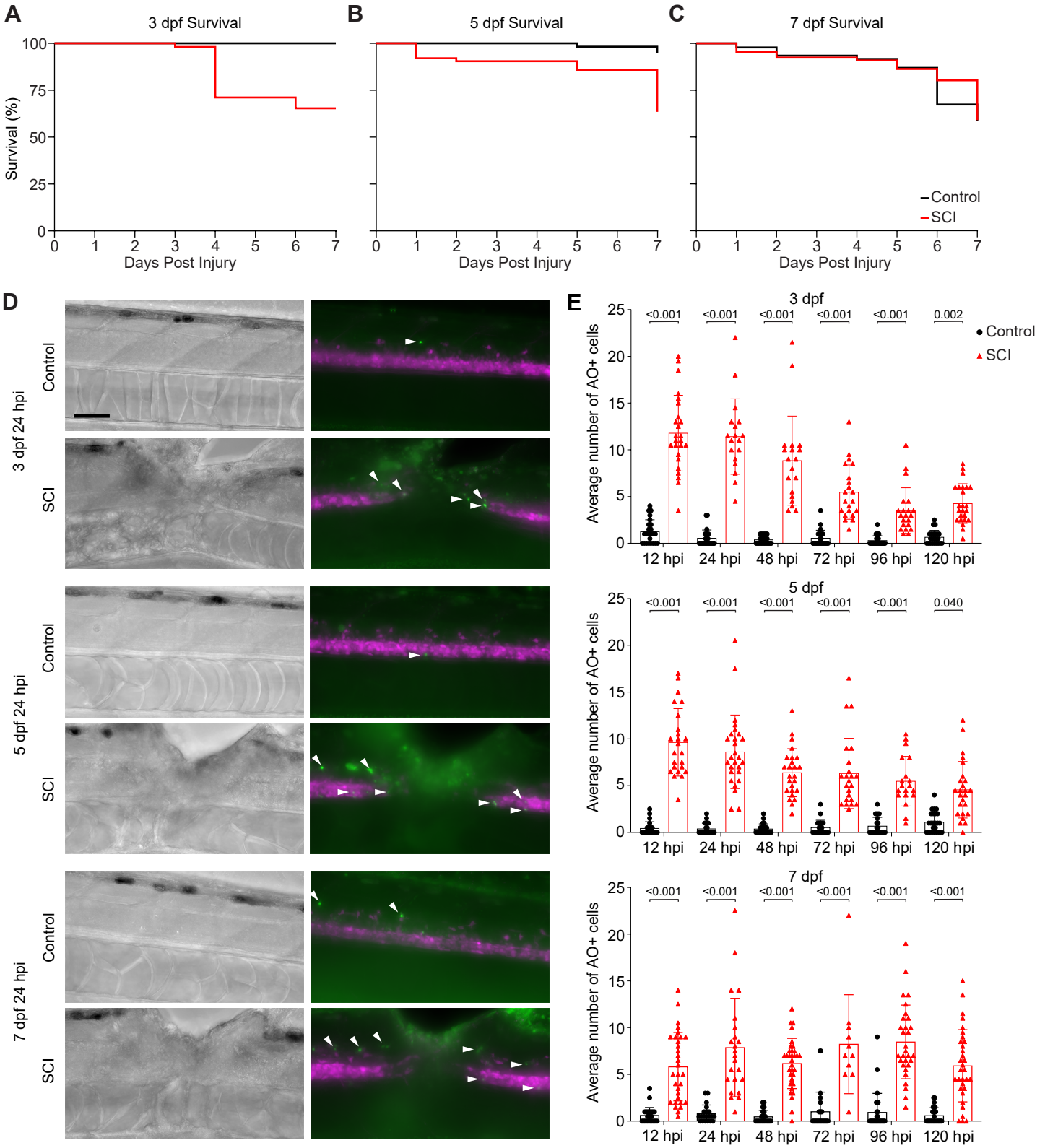
A
3 dpf Survival
Survival (%)
100
75
50
25
0
0 1 2 3 4 5 6 7
Days Post Injury
B
5 dpf Survival
0 1 2 3 4 5 6 7
Days Post Injury
C
7 dpf Survival
Control
SCI
0 1 2 3 4 5 6 7
Days Post Injury
D
3 dpf 24 hpi
Control
SCI
5 dpf 24 hpi
Control
SCI
7 dpf 24 hpi
Control
SCI
E
3 dpf
Control
SCI
Average number of AO+ cells
<0.001 <0.001 <0.001 <0.001 <0.001 0.002
12 hpi 24 hpi 48 hpi 72 hpi 96 hpi 120 hpi
5 dpf
Average number of AO+ cells
<0.001 <0.001 <0.001 <0.001 <0.001 0.040
12 hpi 24 hpi 48 hpi 72 hpi 96 hpi 120 hpi
7 dpf
Average number of AO+ cells
<0.001 <0.001 <0.001 <0.001 <0.001 <0.001
12 hpi 24 hpi 48 hpi 72 hpi 96 hpi 120 hpi

Figure 2

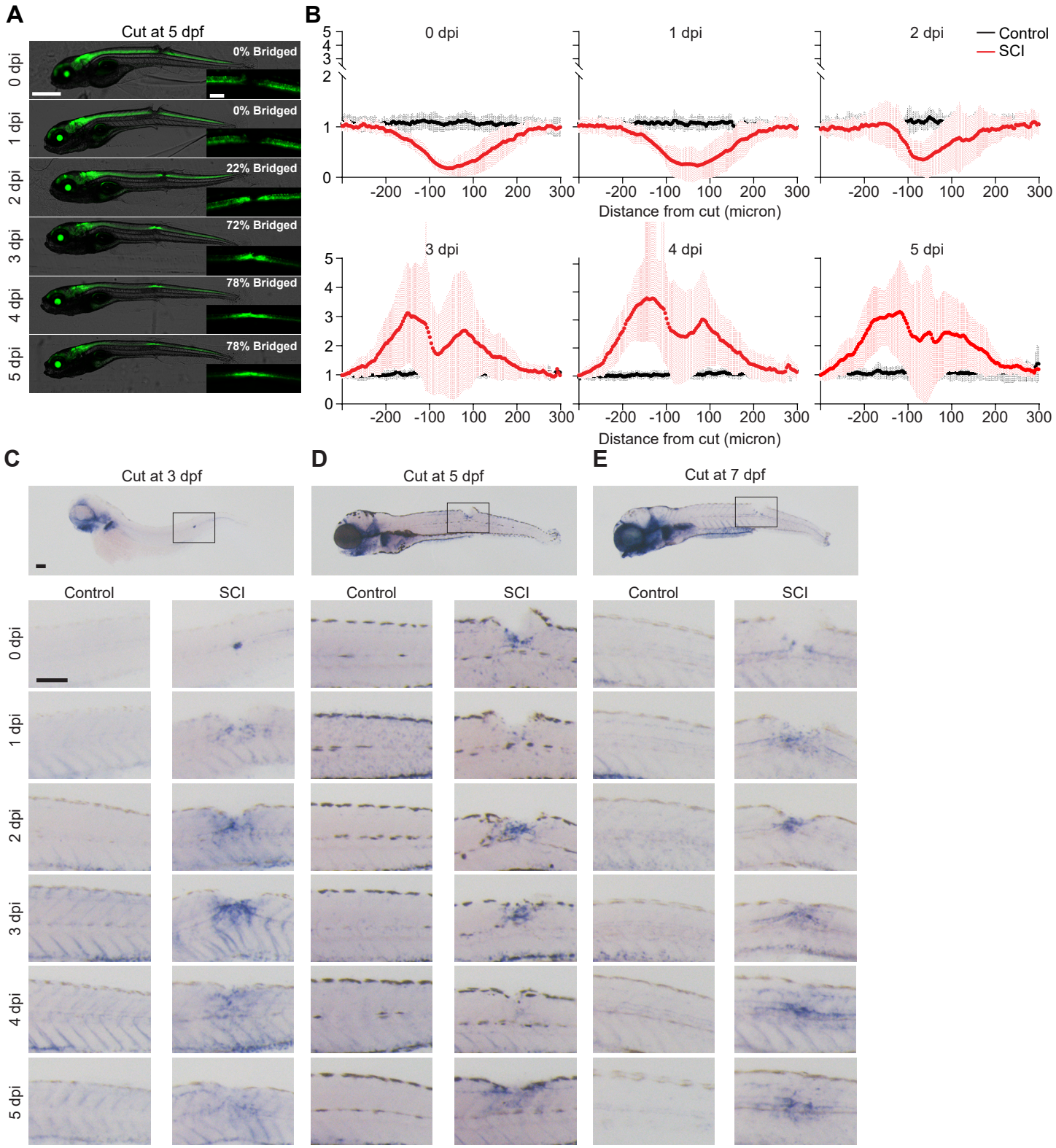
A
Cut at 5 dpf
0 dpi
1 dpi
2 dpi
3 dpi
4 dpi
5 dpi
0% Bridged
0% Bridged
22% Bridged
72% Bridged
78% Bridged
78% Bridged
B
0 dpi
1 dpi
2 dpi
3 dpi
4 dpi
5 dpi
Control
SCI
Distance from cut (micron)
C
Cut at 3 dpf
D
Cut at 5 dpf
E
Cut at 7 dpf
Control
SCI

Figure 3

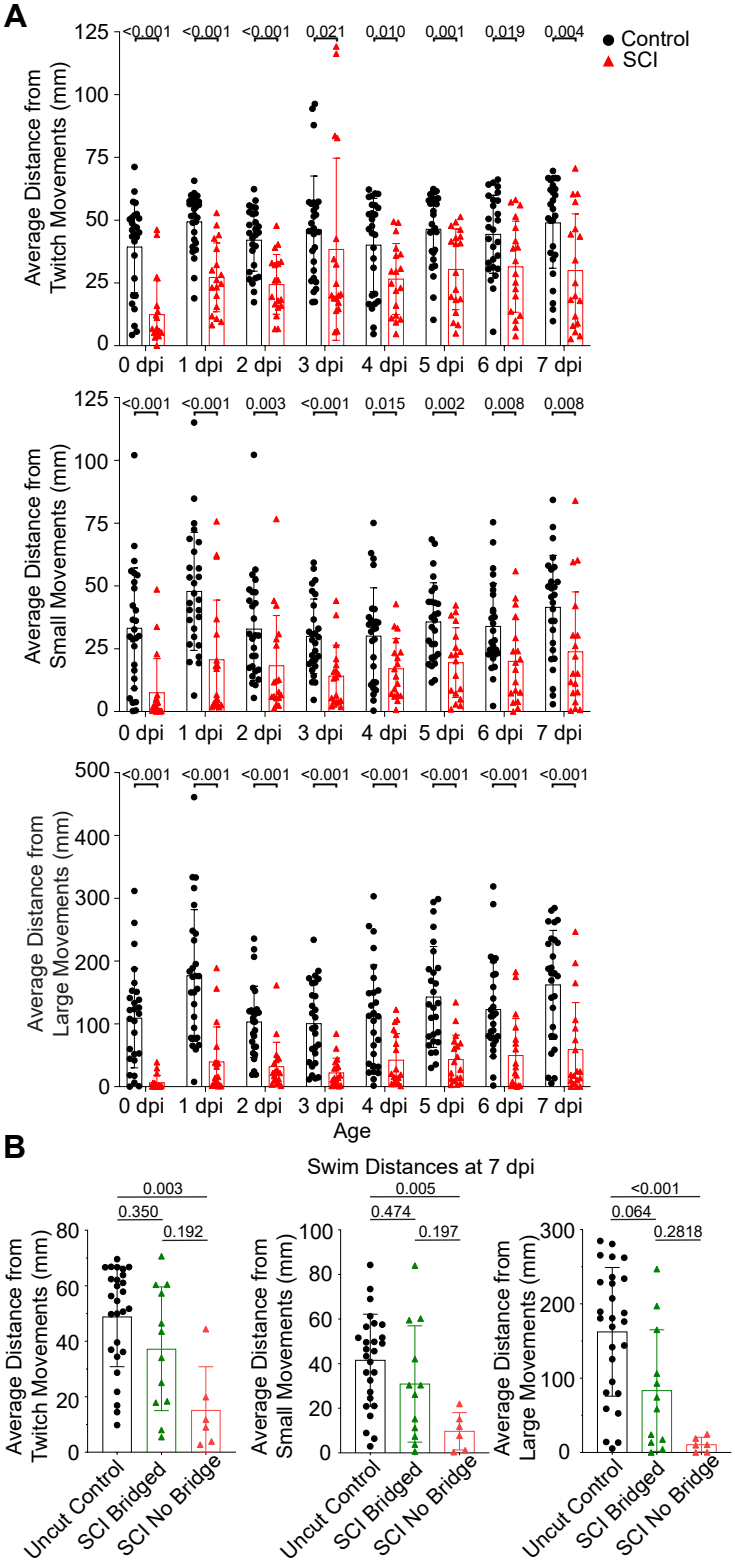
A
Control
SCI
Average Distance from Twitch Movements (mm)
<0.001 <0.001 <0.001 0.021 0.010 0.001 0.019 0.004
Average Distance from Small Movements (mm)
<0.001 <0.001 0.003 <0.001 0.015 0.002 0.008 0.008
Average Distance from Large Movements (mm)
<0.001 <0.001 <0.001 <0.001 <0.001 <0.001 <0.001 <0.001
0 dpi 1 dpi 2 dpi 3 dpi 4 dpi 5 dpi 6 dpi 7 dpi
Age
B
Swim Distances at 7 dpi
Average Distance from Twitch Movements (mm)
0.003
0.350
0.192
Average Distance from Small Movements (mm)
0.005
0.474
0.197
Average Distance from Large Movements (mm)
<0.001
0.064
0.2818
Uncut Control
SCI Bridged
SCI No Bridge

Figure 4

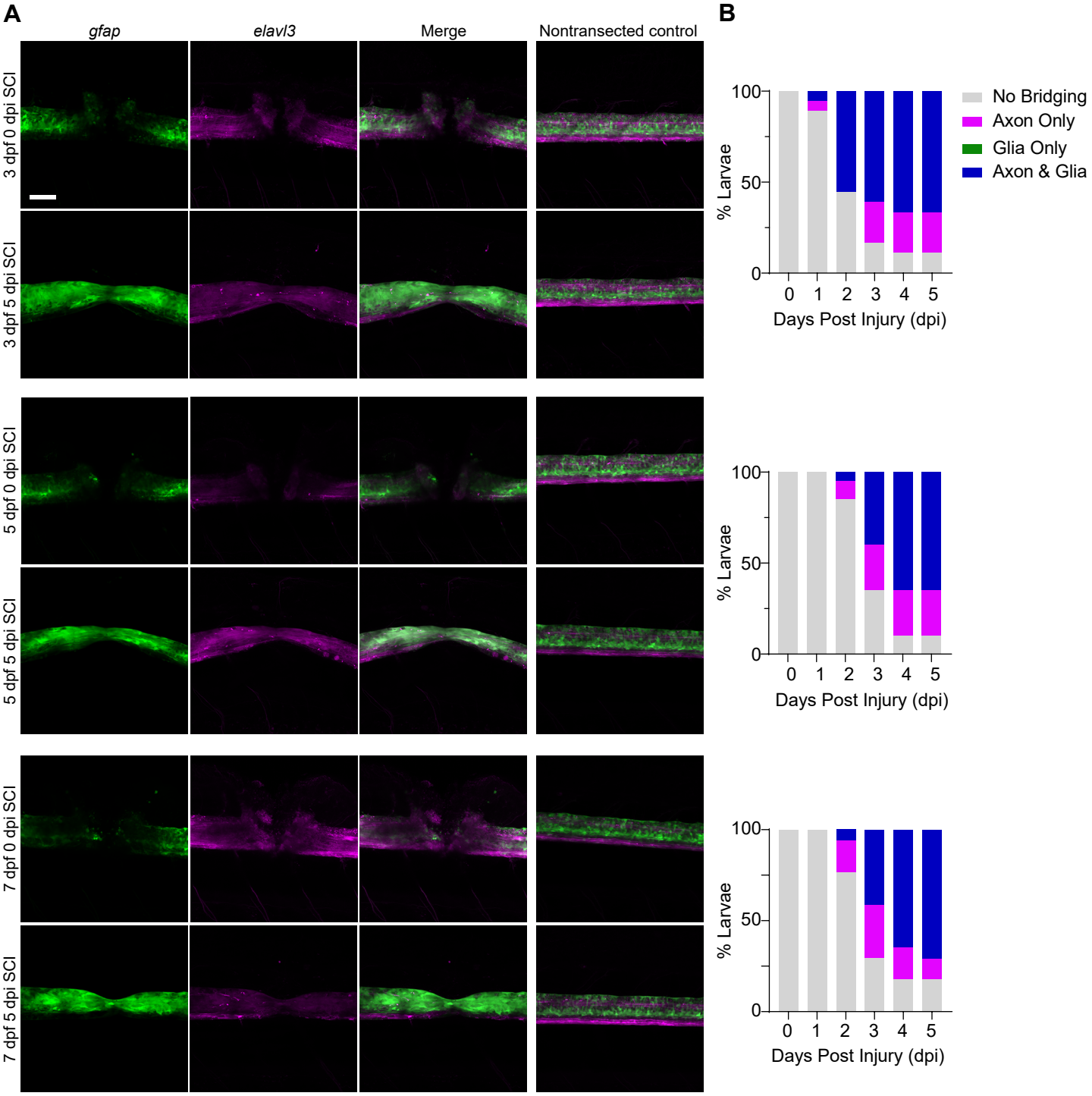
A
gfap
elavl3
Merge
Nontransected control
3 dpf 0 dpi SCI
3 dpf 5 dpi SCI
5 dpf 0 dpi SCI
5 dpf 5 dpi SCI
7 dpf 0 dpi SCI
7 dpf 5 dpi SCI
B
% Larvae
100
50
0
0 1 2 3 4 5
Days Post Injury (dpi)
No Bridging
Axon Only
Glia Only
Axon & Glia